doi: 10.82124/CEAS-GNC-2026-108

CEAS-GNC-2026-108

EuroGNC
Madrid, Spain May 5th-7th 2026

Control Architectures Integrating Direct Lift Capability for Future Aircraft Concepts

João Martins Research Associate, Institute of Aeroelasticity, German Aerospace Center (DLR), Weßling, Germany & Technical University Delft, Delft, The Netherlands.
Joao.DiasMartins@dlr.de

Gertjan Looye Head of Department, Institute of Aeroelasticity & Senior Expert, Institute of Flight Systems, German Aerospace Center (DLR), Weßling, Germany.
Gertjan.Looye@dlr.de

Thiemo Kier Head of Group, Institute of Aeroelasticity, German Aerospace Center (DLR), Weßling, Germany.
Thiemo.Kier@dlr.de

Spilios Theodoulis Associate Professor, Technical University Delft, Delft, The Netherlands.
S.Theodoulis@tudelft.nl

ABSTRACT

Direct Lift Control (DLC) uses control devices at the wing that allow for directly adjusting lift. When properly combined with adjustment of angle of attack, the non-minimum-phase behavior associated with elevator controls is removed, and the load factor response time and disturbance rejection improve considerably. DLC has seen only limited application though, due to the absence of suitable control devices and actuation capability on current wing designs. Future concepts tend to move towards more use of multi-functional control devices along the trailing edge to accommodate for integration of load alleviation and cruise performance optimizing functions. This allows for providing DLC capability by means of a suitable allocation scheme, providing good reasons for its renewed consideration. From this perspective, this work addresses the crucial aforementioned proper integration with angle of attack adjustment to allow for optimal use of DLC. Two architectures are proposed and compared through simulation analyses based on an experimental aircraft intended to demonstrate advanced wing concepts. Hardware-in-the-Loop tests are also performed replacing the DLC control devices and actuation system with a physical control surface system. Both architectures show considerable improvement in handling, disturbance rejection and passenger comfort in comparison with traditional concepts.

Keywords: Direct Lift Control, Flight Control, Multi-functional trailing-edge devices, Control Architecture

Nomenclature

m = Mass
$\mathbf{J}$ = Inertia tensor
V = Airspeed
$\mathbf{V}_b$ = Linear velocity vector on body axes

$\mathbf{\Omega}_b$ = Rotational velocity vector on body axes
u, v, w = Velocity components on body axes
p, q, r = Roll, pitch and yaw rate
ϕ, θ, ψ = Roll, pitch and yaw angles
$\mathbf{u}_f$ = Modal deflection
δ = Control surface deflection
α = Angle of attack
β = Angle of sideslip
γ = Flight path angle
$\mathbf{n}$ = Load factor vector
n_z = Normal load factor
h = Altitude
T, D, L = Thrust, Drag, and Lift forces
M = Moment around the pitch axes
M_h = Hinge Moment
C, Q = Dimensionless coefficients
$\mathbf{P}$ = Loads vector
g = Gravitational constant
q_∞ = Dynamic pressure
S = Reference wing area
c_{ref} = Reference length
$\mathbf{\Phi}$ = Eigenvector matrix
$\mathbf{x}$ = State vector
s = Laplace variable
ω_n = Natural frequency
ζ = Damping ratio
K = Controller gain

1 Introduction

For the longitudinal dynamics of an aircraft, the normal load factor (n_z) is a very intuitive variable for pilots to control. By using the stick, pilots are able to pull it to produce vertical accelerations and change the aircraft's vertical velocity, and by releasing it the aircraft would maintain a constant flight path angle and vertical speed. This would mean that the pilot would only need to intervene when a disturbance would deviate the flight path angle from its desired course. This is the idea behind most vertical flight controllers. The general idea consists of changing lift by pitching the aircraft using the elevators to modify the angle of attack (AoA). Due to the required build up of AoA to influence lift, especially at low speeds, this method is slow and originates a non-minimum-phase behavior in the vertical dynamics of aircraft. It is for this reason that it is more common to use C* as a commanded variable, as it complements initial response by using pitch rate [1, 2].

Direct Lift Control (DLC) triggers immediate response of the normal load factor in the intended direction, allowing for direct use as a commanded variable. DLC allows for directly controlling and intentionally influencing the lift of fixed-wing aircraft, while ideally not changing the moments around the aircraft's axes [3]. This is achieved by deflecting control surfaces located close to the center of gravity (CG) of the aircraft. These are typically relatively fast trailing edge devices or spoilers located on the aircraft's main wing. Because of its principle, DLC offers a fast way to control the vertical dynamics of aircraft and it allows decoupling, to some extent, of its pitch and heave dynamics. DLC also removes the non-minimum-phase behavior present when only elevators are used to control the vertical dynamics of aircraft since it can directly accelerate the aircraft in its intended direction. Moreover, because of this direct influence to the aircraft's lift, wind disturbances like gust or turbulence encounters can be handled significantly better. Conventional longitudinal controllers require pitch corrections to handle these disturbances, while DLC can directly counteract the variation of lift caused by these. This results in significantly better passenger comfort levels on aircraft with DLC capabilities [4–6].

Although DLC possesses the aforementioned advantages, the vertical dynamics of an aircraft cannot be controlled solely using DLC. Control surface deflection limits impose an upper bound on achievable lift variation. Additionally, constant use of these devices create variations of drag which would be uncomfortable for passengers [4, 7]. These reasons motivate a coordinated approach between DLC and the use of elevators to control n_z [6, 8]. This approach retains the short-term advantages of DLC without the drawbacks associated with its long-term use.

Despite the benefits of incorporating DLC capabilities into aircraft, not many applications of it exist. Relevant examples of DLC applications are the Lockheed L-1011 Tristar and the Embraer 190 series equipped with steep approach mode. Although the Lockheed L-1011 Tristar did not possess a Fly-By-Wire (FBW) system and the DLC coordination during the flight approach phase was done by the pilot, studies on its landing system show touchdown performance and passenger comfort improvements, and greater pilot acceptability [9, 10]. More specifically, when DLC capabilities were considered, touchdown longitudinal dispersion was reduced by 50%, pitch correction was considerably lower, descent rate at touchdown was reduced by a factor of two, and accelerations were reduced by 50% leading to a significantly higher ride comfort [5]. More recently, the US navy has re-introduced large-scale implementation of DLC as part of its Maritime Augmented Guidance with Integrated Control for Carrier Approach and Recovery Precision Enabling Technologies (MAGIC CARPET), which aims to increase carrier landing's safety and performance by using DLC. Similarly, the DLC implementation on the military aircraft also showed positive results. Its independent but coordinated pitch and vertical path control allowed for massive flight path tracking improvements and a significant reduction of pilot workload during carrier landings [6].

The bigger difficulty that DLC faced to become more popular has been the lack of aircraft with the relevant devices allowing DLC implementations to be deployed on its flight computer. With the move towards more sustainable aircraft designs, bigger aspect ratio wings are being considered due to their significant reduction of induced drag [11]. Along with higher aspect ratio wings, new wing designs have multi-functional trailing edge (MFTE) devices to accommodate load alleviation and cruise performance optimizing control functions [12]. With the availability of these devices and assuming sufficient actuation capabilities, DLC can be provided via control architecture modifications. Therefore, with FBW systems now standard and new wing design concepts incorporating already available MFTE devices, DLC can offer significant benefits compared to traditional control of the vertical dynamics via the elevators, without requiring hardware changes to the aircraft.

Recent work has shown the properties of DLC and how to exploit control surfaces selection for this purpose [4, 13]. Regarding actual DLC implementation strategies and studies on them, apart from DLR's flying test-bed ATTAS, this has not been properly addressed in research [8]. Therefore, in this work, architectural strategies for DLC flight controllers are proposed and discussed in detail. The research focus will be on the design of these architectures to achieve the benefits of DLC while avoiding its inherent limitations. This concerns how to achieve proper coordination between short-term DLC use and long-term adjustment of angle of attack to optimally integrate DLC in a FBW pitch control function. For this, preliminary data of a recently developed flying demonstrator based on a heavily modified business jet with the main wing from the eXtra Performance Wing Project will be used to generate the aircraft model to validate the control architectures in simulation. Additionally, harware-in-the-loop (HiL) tests are performed to illustrate the viability of using certain control surfaces for DLC implementations.

This paper is organized in the following way. Section 2 explains the concepts behind DLC and its properties by making use of a simple point mass model of a fixed-wing aircraft. In section 3, a brief description of the modified Cessna Citation VII aircraft is given. A complete flight dynamic model used for the aircraft simulations is described and a simpler linear model is also presented. In section 4, two proposed architectures using DLC are thoroughly explained and discussed about. Section 5 presents the tracking performance in simulation for both DLC architectures, an analysis on non-minimum-phase behavior, and a comparison between both DLC architectures and another without DLC capabilities under turbulent wind fields. This section ends by showing HiL results. In section 6, concluding remarks and future work are presented.

2 Direct Lift Control Principles

To more easily understand the basic DLC principles, a simple longitudinal point-mass model of a fixed-wing aircraft is taken [14]:

$$m\dot{V} = T - D - mg\sin\gamma \tag{1}$$

$$mV\dot{\gamma} = L - mg\cos\gamma\ . \tag{2}$$

From equation (2) an approximation for n_z can be deduced for small flight path angle values:

$$n_z \approx 1 + \frac{V\dot{\gamma}}{g}\ . \tag{3}$$

From equation (3), assuming constant velocity, the only way to change n_z is for the derivative of the flight path angle, $\dot{\gamma}$, to be modified. Equation (2) shows that $\dot{\gamma}$ is changed by increasing or decreasing the lift force. Given that in traditional fixed-wing aircraft the lift force can be written as:

$$L \approx q_\infty S\left(C_{L_0} + C_{L_\alpha}\alpha\right)\ , \tag{4}$$

the main way to modify lift is to change AoA. The symbol q_∞ denotes the dynamic pressure. Additionally, the most effective way to change AoA while maintaining the speed constant is to make use of moment generating control surfaces like the elevators to generate a pitch moment to initiate this maneuver. Although it is the conventional way of controlling n_z, this method is not direct. This can be understood by inspecting how an elevator deflection propagates through the aircraft dynamics [4]:

$$\underbrace{\Delta\delta_{\text{ele}} \rightarrow \Delta L_{\text{tailplane}} \rightarrow \Delta M \rightarrow \dot{q}}_{\text{instantaneous}} \xrightarrow{\int} \underbrace{\dot{\theta} \xrightarrow{\approx} \dot{\alpha}}_{\text{instantaneous}} \xrightarrow{\int} \underbrace{\Delta\alpha \rightarrow \Delta L \rightarrow \dot{\gamma} \rightarrow n_z}_{\text{instantaneous}}\ . \tag{5}$$

Equation (5) shows that the two integration steps cause a time delay from elevator deflection and the resulting change in n_z. Additionally, because the elevators are behind the CG of the aircraft, the control forces needed to generate the required moment are always opposite to the intended direction of acceleration. Because of the delay and this property of the elevators' location, a non-minimum-phase behavior in the longitudinal dynamics arises. This is undesirable since control design of non-minimum-phase systems is more challenging and there are performance limitations associated with them [15].

On the other hand, DLC offers a faster way of controlling n_z and the possibility of removing the non-minimum-phase behavior. This is achieved using control surfaces closely located to the CG and with minimal influence on the aircraft's moments. With an appropriate choice of control surfaces for DLC purposes, its influence on the dynamics can be expressed as follows [4, 8]:

$$\underbrace{\Delta\delta_{\text{dlc}} \rightarrow \Delta L \rightarrow \dot{\gamma} \rightarrow n_z}_{\text{instantaneous}} \ . \tag{6}$$

This direct link from DLC control surfaces to n_z dynamics may allow for improvements in its tracking properties and overall vertical response of aircraft. An obvious improvement comes from the removal of the time integration delay in equation (5). Moreover, ΔL acts in the intended direction of acceleration. This can be used to remove the non-minimum-phase behavior of equation (5). Lastly, this direct link to the aircraft's total lift can also be used to improve wind disturbance rejection. Considering the influence from DLC control surfaces, equation (4) can be rewritten as:

$$L \approx q_\infty S \left(C_{L_0} + C_{L_\alpha}\alpha + C_{L_{\delta_{\text{dlc}}}}\delta_{\text{dlc}} \right) \ . \tag{7}$$

Equation (7) shows that DLC control surface deflections appears on the same level as AoA. Therefore, any wind disturbance, α_w, affecting the total AoA can be rapidly compensated using δ_{dlc} or even directly counteracted when an estimate of α_w is available.

As outlined in section 1, DLC is undesirable for use in sustaining a steady state, as this causes additional drag and authority will quickly run out as dynamic pressure changes. For this reason, AoA (and thus elevator) remains the variable of choice for aircraft trim. This poses the architectural challenge of properly coordinating both means of control.

3 Aircraft Platform and Modeling

This work is based on application to a Cessna Citation VII aircraft. An integrated aeroelastic and flight dynamics model was developed based on preliminary geometry and structural data using an in-house modelling process [16]. Images of the modified aircraft can be seen in [17]. There are 26 trailing edge devices spanning across the main wing. Out of those, four of them are ailerons, two on each side. The remaining 22 are MFTE devices. These are responsible for different functions. For DLC purposes, only the most inboard MFTE devices are used. The aircraft has a T-tail configuration with two elevators on the tailplane. These will be responsible for controlling the pitch dynamics.

The model used for simulating the aircraft has 6 degrees of freedom (DoF) from rigid-body motion plus the DoF from aeroelastic dynamics. The theory used to model the aircraft dynamics with its aeroelastic contribution was developed in Ref. [16]. Its mathematical representation are the (nonlinear) equations of motion (EOM) based on mean body-reference axes [16, 18]:

$$\begin{aligned} \begin{bmatrix} m_b \left(\dot{\mathbf{V}}_b + \mathbf{\Omega}_b \times \mathbf{V}_b - \mathbf{T}_{bE}\mathbf{g}_E \right) \\ \mathbf{J}_b \dot{\mathbf{\Omega}}_b + \mathbf{\Omega}_b \times (\mathbf{J}_b \mathbf{\Omega}_b) \end{bmatrix} &= \mathbf{\Phi}_{gb}^T \mathbf{P}_g^{\text{ext}} \\ \mathbf{M}_{ff}\ddot{\mathbf{u}}_f + \mathbf{B}_{ff}\dot{\mathbf{u}}_f + \mathbf{K}_{ff}\mathbf{u}_f &= \mathbf{\Phi}_{gf}^T \mathbf{P}_g^{\text{ext}} \ . \end{aligned} \tag{8}$$

The subscripts b and f indicate whether a variable is related to the rigid-body or to the flexible motion. The first equation expresses the rigid-body motion (b-set), while the second one expresses the flexible motion (f-set). The rigid-body motion is described using the linear and rotational aircraft's velocity. The gravity contribution is achieved by using $\mathbf{g}_E$ in vector form in the earth inertial frame. A coordinate system transformation matrix $\mathbf{T}_{bE}$ is used to go from the earth to the body's frame axes. The flexible motion is described using the modal matrices of mass $\mathbf{M}_{ff}$, damping $\mathbf{B}_{ff}$ and stiffness $\mathbf{K}_{ff}$. The external forces $\mathbf{P}_g^{\text{ext}}$ are given in the g-set (structural set). These are external forces originated from aerodynamics, gusts, and thrust. Lastly, $\mathbf{\Phi}_{gb}$ and $\mathbf{\Phi}_{gf}$ are eigenvector matrices that convert loads from the rigid-body and flexible sets to the modal domain.

Note that different sources for $\mathbf{P}_g^{\text{ext}}$ were mentioned. More particularly, one source that is relevant for control is the control surfaces influence on the aircraft dynamics. It is important to understand that control surface deflections affect the dynamics in equation (8) via $\mathbf{P}_g^{\text{ext}}$.

Regarding the model used for controller design, since the rigid-body motion is crucial for it, some simplifications are made to the model in equation (8). The main simplification was assuming a quasi-static aeroelastic behavior. In particular, the time derivatives of the modal deflections, $\dot{\mathbf{u}}_f$ and $\ddot{\mathbf{u}}_f$ are neglected, allowing the second equation of (8) to be solved for $\mathbf{u}_f$. With modal deflection dynamics removed from the model, and since the control surface influence is linear, equation (8) can be rewritten in the standard form for control design:

$$\dot{\mathbf{x}} = \mathbf{f}\left(\mathbf{x}, \mathbf{u}\right) + \mathbf{g}\left(\mathbf{x}\right) \boldsymbol{\delta} \; . \tag{9}$$

In equation (9), $\mathbf{x}$ denotes the state vector containing the internal states of the aircraft, $\boldsymbol{\delta}$ is the vector of the control surface deflections, and $\mathbf{f}$ and $\mathbf{g}$ are nonlinear functions obtained from a rearrangement of equation (8). These aeroelastic simplifications were only performed for control law derivations, while the full aircraft model was retained for all closed-loop (CL) analyses.

To examine the removal of the non-minimum-phase behavior, a simplified linear model is employed to investigate the elimination of the Right-Half-Plane (RHP) zero. The analysis is only relevant immediately after control input changes. Airspeed magnitude V_0 is assumed to be constant and the focus is placed on the AoA, pitch and flight path angle dynamics for small values around an initial equilibrium position. The stability derivatives are assumed constant. A standard longitudinal linear model for the aircraft dynamics is taken with control inputs from elevator deflections, δ_{ele}, and DLC control surface deflections, δ_{dlc}. Additionally, the AoA wind disturbance, α_w, is also added as an input disturbance to the AoA with no wind influence, α_i. The simplified model is written in equation (10):

$$\begin{cases} \dot{\alpha}_i = q + \dfrac{q_\infty S}{m_b V_0} \left(C_{Z_q} \dfrac{c_{\text{ref}}}{V_0} q + C_{Z_\alpha} \alpha + C_{Z_{\delta_{\text{ele}}}} \delta_{\text{ele}} + C_{Z_{\delta_{\text{dlc}}}} \delta_{\text{dlc}} \right) \\ \dot{q} = \dfrac{q_\infty S c_{\text{ref}}}{J_{yy}} \left(C_{m_q} \dfrac{c_{\text{ref}}}{V_0} q + C_{m_\alpha} \alpha + C_{m_{\delta_{\text{ele}}}} \delta_{\text{ele}} + C_{m_{\delta_{\text{dlc}}}} \delta_{\text{dlc}} \right) \\ \dot{\theta} = q \\ \gamma = \theta - \alpha_i \\ \alpha = \alpha_i + \alpha_w \\ n_z = -\dfrac{q_\infty S}{m_b g} \left(C_{Z_q} \dfrac{c_{\text{ref}}}{V_0} q + C_{Z_\alpha} \alpha + C_{Z_{\delta_{\text{ele}}}} \delta_{\text{ele}} + C_{Z_{\delta_{\text{dlc}}}} \delta_{\text{dlc}} \right) \; . \end{cases} \tag{10}$$

4 Direct Lift Control Architecture Design

Two proposed architectures for DLC are presented and discussed in this section. The DLC architectures are combined with a Nonlinear Dynamic Inversion (NDI) controller. This enables greater generalization and facilitates the transformation from commanded pitch rate to commanded elevator deflection allowing the DLC architectures to be tested without requiring dedicated inner-loop control laws [19–21]. The complete vertical dynamics control diagram is illustrated in Fig. 1.

The overall idea behind both architectures presented in section 4.1 and 4.2 is: use the DLC control surfaces to create a fast n_z response, while using the AoA to track the desired n_z in the long-term and

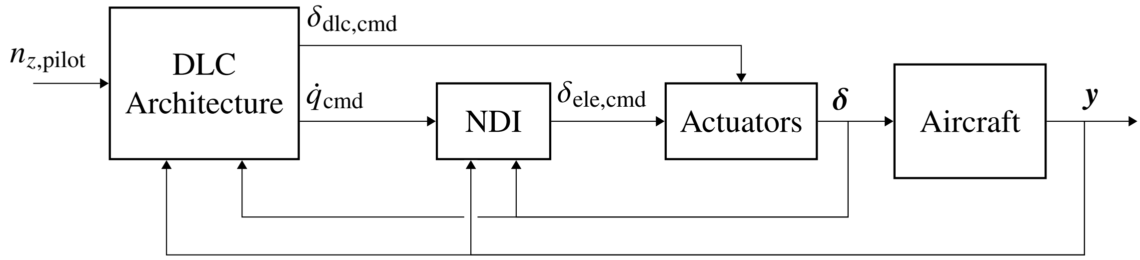

Fig. 1 Vertical dynamics control diagram.

returning the DLC control surfaces back to their initial position after reaching an equilibrium. This is achieved by generating two control paths as shown in Fig. 1: the commanded DLC control surface deflection, $\delta_{\text{dlc,cmd}}$, and the commanded pitch rate, $\dot{q}_{\text{cmd}}$. The latter is mapped to commanded elevator deflections, $\delta_{\text{ele,cmd}}$, using a NDI function. The DLC architecture is responsible for creating these paths and ensuring that the short- and long-term properties are achieved.

For the design of these architectures, an equation for n_z is required. This is obtained from equation (8) with the appropriate aeroelastic simplifications discussed in section 3. From its definition, the left side of the first three equations of (8) are related to the load factor $\mathbf{n}$:

$$m_b \left(\dot{\mathbf{V}}_b + \mathbf{\Omega}_b \times \mathbf{V}_b - \mathbf{T}_{bE} \mathbf{g}_E \right) = -m_b g \cdot \mathbf{n} \, . \tag{11}$$

The first three elements of the right side of equation (8) are the components of the external force vector on the body axes. Naming this force vector $\mathbf{F}_b$ and noting it is a function of internal aircraft states, equation (11) is rewritten:

$$\mathbf{n} = -\frac{1}{m_b g} \mathbf{F}_b \left(q_\infty, \alpha, \beta, \mathbf{\Omega}_b, \boldsymbol{\delta} \right) \, . \tag{12}$$

Since only the normal load factor is relevant for DLC, only the z-component of equation (12) is required:

$$\begin{aligned} n_z = -\frac{q_\infty}{m_b g} \Big(& Q_{z_0} + Q_{z_\alpha} \alpha + Q_{z_\beta} \beta + Q_{z_p} \frac{c_{\text{ref}}}{V} p + Q_{z_q} \frac{c_{\text{ref}}}{V} q + Q_{z_r} \frac{c_{\text{ref}}}{V} r + \\ & + \mathbf{Q}_{z_{\delta_{\text{dlc}}}} \boldsymbol{\delta}_{\text{dlc}} + \mathbf{Q}_{z_{\delta_{\text{ele}}}} \boldsymbol{\delta}_{\text{ele}} + \mathbf{Q}_{z_{\delta_{\text{rem}}}} \boldsymbol{\delta}_{\text{rem}} \Big) \, , \end{aligned} \tag{13}$$

$$n_z = n_z^0 + n_z^\alpha + n_z^\beta + n_z^p + n_z^q + n_z^r + n_z^{\text{dlc}} + n_z^{\text{ele}} + n_z^{\text{rem}} \, , \tag{14}$$

where the various Q_z's are dimensionless coefficients based on aerodynamic data, and the control surfaces were expanded to have explicitly the contributions from DLC (dlc), elevators (ele), and remaining (rem) control surfaces.

From equation (13) it can be seen that n_z is directly influenced by AoA and $\boldsymbol{\delta}_{\text{dlc}}$. Accurate tracking of n_z would thus require exact setting of both variables, as well as perfect knowledge of the related aerodynamic coefficients. For this reason, a control loop is applied that combines direct feedforward for fast response with integral feedback to allow for compensating the aforementioned potential mismatches. The resulting $n_{z,\text{cmd}}$ is subsequently distributed between and realized by AoA and $\boldsymbol{\delta}_{\text{dlc}}$. This control loop is illustrated in Fig. 2.

The parameter K_{fb} controls how much the integral of the error is fed through. Choosing this parameter excessively large, the n_z response will exhibit an oscillatory behavior. This parameter should be used and chosen solely for removing steady-state errors and improve slightly tracking performance. This

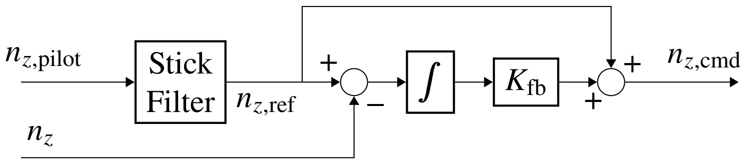

Fig. 2 Normal load factor control law.

control law allows n_z feedback to be incorporated and ensure zero n_z steady-state error in the presence of model mismatches and disturbances. Note that this architecture can be extended with feed-forward of (estimated) disturbance terms in order to directly cancel resulting lift contributions as demonstrated in [7].

4.1 Offload Architecture

In this "offload" controller architecture, the idea is to make the DLC control surfaces the primary responsibles for tracking $n_{z,\text{cmd}}$, while using an integrator to offload this responsibility towards AoA, very much like how elevator control is often transferred to the stabilizer [22]. In Fig. 3, a diagram of this controller architecture is presented.

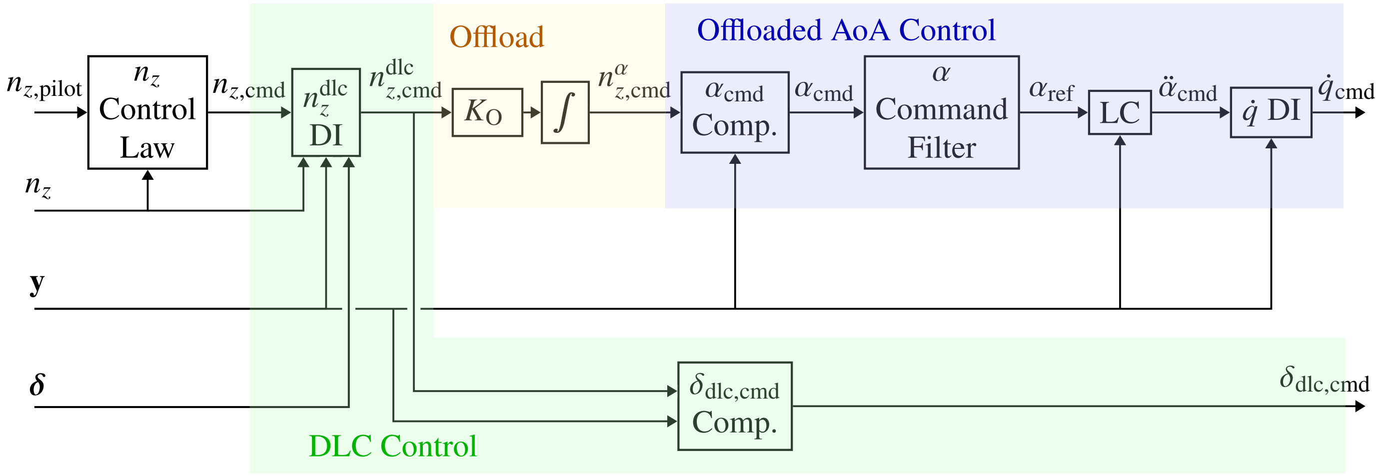

Fig. 3 Offload controller architecture

As it is shown in Fig. 3, an integrator with a constant K_O is central to the architecture and is responsible for offloading n_z tracking responsibility. The measured normal load factor, n_z, was made explicit in the diagram while the remaining measured signals were grouped in $\mathbf{y}$ to simplify the diagram.

The "n_z Control Law" block was presented in Fig. 2. The "n_z^{dlc} DI" block performs a dynamic inversion (DI) to obtain the commanded n_z contribution from DLC control surfaces. Using equation (14) and since the concept of this architecture is for DLC control surfaces to track entirely n_z, the relation between $n_{z,\text{cmd}}$ and the commanded DLC contribution $n_{z,\text{cmd}}^{\text{dlc}}$, is found as:

$$n_{z,\text{cmd}} = n_z^0 + n_z^\alpha + n_z^\beta + n_z^p + n_z^q + n_z^r + n_z^{\text{ele}} + n_z^{\text{rem}} + n_{z,\text{cmd}}^{\text{dlc}} \,. \tag{15}$$

Rearranging equation (15) and using the measurement for n_z, a simpler equation for $n_{z,\text{cmd}}^{\text{dlc}}$ is found:

$$
\begin{aligned}
n_{z,\text{cmd}}^{\text{dlc}} &= n_{z,\text{cmd}} - \left(n_z - n_z^{\text{dlc}}\right) \\
&= n_{z,\text{cmd}} - \left(n_z + \frac{q_\infty}{m_b g}\mathbf{Q}_{z_{\boldsymbol{\delta}_{\text{dlc}}}}\boldsymbol{\delta}_{\text{dlc}}\right) .
\end{aligned}
\tag{16}
$$

To implement equation (15), measurements of AoA, sideslip, angular rates and of all control surface deflections are required. Using the implementation of equation (16), only n_z and $\boldsymbol{\delta}_{\text{dlc}}$ are necessary. Furthermore, using the measurement of n_z has the advantage of accounting for disturbances and contributions that are not modeled in equation (15). However, using the n_z measurement requires careful filtering to it due to high frequency flexible dynamics. To counteract the loss of bandwidth and phase margin from filtering the measured signal, a complementary filter should be used for n_z where a measurement for low frequencies and a model-based estimation for high frequencies are combined. Equation (16) is implemented in "n_z^{dlc} DI".

After obtaining $n_{z,\text{cmd}}^{\text{dlc}}$, this is directly used to compute $\boldsymbol{\delta}_{\text{dlc,cmd}}$. If $\boldsymbol{\delta}_{\text{dlc}}$ is multi-dimensional, a control allocation strategy is required to correctly command $\boldsymbol{\delta}_{\text{dlc,cmd}}$. Assuming a simple control allocation method of the form $\boldsymbol{\delta}_{\text{dlc,cmd}} = \mathbf{A}u_{\text{dlc,cmd}}$, where $\mathbf{A}$ is a constant column vector and $u_{\text{dlc,cmd}}$ is a scalar representing a virtual control input for DLC, the commanded values for the DLC control surfaces become:

$$
\boldsymbol{\delta}_{\text{dlc,cmd}} = \mathbf{A}\left(-\frac{q_\infty}{m_b g}\mathbf{Q}_{z_{\boldsymbol{\delta}_{\text{dlc}}}}\mathbf{A}\right)^{-1} n_{z,\text{cmd}}^{\text{dlc}} . \tag{17}
$$

In the "$\boldsymbol{\delta}_{\text{dlc,cmd}}$ Computation" block, equation (17) is implemented. In the center of the diagram shown in Fig. 3 highlighted in yellow, is the integrator offloading the commanded DLC contribution to commanded AoA contribution:

$$
n_{z,\text{cmd}}^{\alpha} = \int K_O n_{z,\text{cmd}}^{\text{dlc}} dt . \tag{18}
$$

The gain K_O determines how fast the dynamics are being offloaded from DLC control surfaces to AoA. Since the AoA is controlled using the elevators resulting in slower dynamics compared to DLC control surfaces, an appropriate choice for K_O is crucial for the correct functioning of this architecture. Choosing it large, fast dynamics are allowed to go through. However, due to the slower pitching dynamics, the AoA would not be able to track the fast commanded n_z dynamics, resulting in a faster outer-loop and slower inner-loop. Oscillations and possible instabilities are expected if K_O is chosen too large. By selecting smaller values of K_O, only slow dynamics are passed through the integrator, resulting in the desired behavior where DLC control surfaces operate at higher frequencies, while AoA and elevators track the slower dynamics of n_z. Choosing it too small results in the DLC control surfaces becoming the primary inputs controlling the vertical dynamics and increasing its control activity.

Lastly, for the offloaded AoA control, $\dot{q}$ is used for controlling the AoA dynamics. This involves computing $\dot{q}_{\text{cmd}}$ from $n_{z,\text{cmd}}^{\alpha}$. To do this, the commanded AoA is first obtained with the "α_{cmd} Comp." block, where "Comp." denotes computation. Similarly to the DLC control surfaces in equation (17), the commanded AoA can be found as:

$$
\alpha_{\text{cmd}} = \left(-\frac{q_\infty}{m_b g}Q_{z_\alpha}\right)^{-1} n_{z,\text{cmd}}^{\alpha} . \tag{19}
$$

To control AoA using $\dot{q}$, a differential equation relating them is required. From its definition:

$$\dot{\alpha} = \frac{\dot{w}u - \dot{u}w}{u^2 + w^2} \approx \frac{\dot{w}}{V} \ . \tag{20}$$

In equation (20), $w \ll u$, $u \approx V$ and $\dot{u}w \ll V^2$ were assumed. For highly maneuverable aircraft, such as fighter jets, some of these assumptions may not be reasonable. In such cases, the full expression in equation (20) must be used, resulting in a more complex differential equation. However, since the present work does not consider such applications, these assumptions are retained. Using equation (11) to expand the time derivative of w, equation (20) can be written as:

$$\dot{\alpha} \approx \frac{1}{V}\left(qV - pv + \cos(\phi)\cos(\theta)g - gn_z\right) \ . \tag{21}$$

To obtain the $\dot{q}$ influence on the AoA dynamics, equation (21) needs to be differentiated once. While doing this, many of the terms present in equation (21) can be simply neglected due to their null or very small influence to the resulting $\ddot{\alpha}$ dynamics. The longitudinal approximated $\ddot{\alpha}$ dynamics become:

$$\ddot{\alpha} \approx \frac{1}{V}\left(\dot{q}V - g\dot{\theta}\sin(\theta) + \frac{q_\infty}{m_b}\left(\mathbf{Q}_{z_\delta}\dot{\boldsymbol{\delta}} + Q_{z_\alpha}\dot{\alpha} + Q_{z_q}\frac{c_{\text{ref}}}{V}\dot{q}\right)\right) \ . \tag{22}$$

To obtain an equation for the commanded $\dot{q}$, equation (22) can be inverted and solved for it, generating a NDI controller for the AoA dynamics. This is presented in equation (23):

$$\dot{q}_{\text{cmd}} = \left(1 + \frac{q_\infty}{m_b}Q_{z_q}\frac{c_{\text{ref}}}{V^2}\right)^{-1}\left(\ddot{\alpha}_{\text{cmd}} - \frac{1}{V}\left(-g\dot{\theta}\sin(\theta) + \frac{q_\infty}{m_b}\left(\mathbf{Q}_{z_\delta}\dot{\boldsymbol{\delta}} + Q_{z_\alpha}\dot{\alpha}\right)\right)\right) \tag{23}$$

This equation is implemented in the "$\dot{q}$ DI" block. To obtain the variable $\ddot{\alpha}_{\text{cmd}}$ a linear compensator (LC) and an α command filter are required. The "LC" block implements a linear controller to stabilize the cascaded inverted dynamics:

$$\ddot{\alpha}_{\text{cmd}} = \left(K_p + K_i\frac{1}{s}\right)(\alpha_{\text{ref}} - \alpha) + K_d\left(\dot{\alpha}_{\text{ref}} - \dot{\alpha}\right) + \ddot{\alpha}_{\text{ref}} \ . \tag{24}$$

The "α Command Filter" block implements the second order filter shown in equation (25):

$$\alpha_{\text{ref}} = \frac{\omega_{n,o}^2}{s^2 + 2\zeta_o\omega_{n,o}s + \omega_{n,o}^2}\alpha_{\text{cmd}}. \tag{25}$$

The parameters of this command filter should be chosen according to the desired AoA response. Additionally, since this command filter determines the bandwidth of the AoA dynamics, it should be tuned in accordance with the offloaded dynamics. If the bandwidth of the command filter is too small, the AoA dynamics cannot track the commanded values from the offloaded dynamics, resulting in oscillatory behavior. Therefore, the command filter bandwidth should be chosen as fast as the offloaded dynamics to minimize oscillations.

4.2 Complementary Filter Bank Architecture

The second developed architecture achieving DLC capabilities is presented in this section. For this architecture, ideas from Ref. [8] were considered. There, a command filter was used for the AoA and the error between the measured and unfiltered signal was utilized to command DLC control surface deflection values. Therefore, the DLC control surfaces controlled the lift variations that the AoA could not achieve due to its slower dynamics.

Similarly, the architecture proposed here uses a low- and high-pass filter, which will be denoted as a complementary filter bank (CFB), to separate the commanded n_z contributions into different frequencies. The low-pass signal is tracked with AoA, while the high-pass signal with the DLC control surfaces. By ensuring that the sum of the two existing filters in the CFB is 1, no commanded n_z information is filtered out. In Fig. 4, a diagram of the proposed architecture is presented.

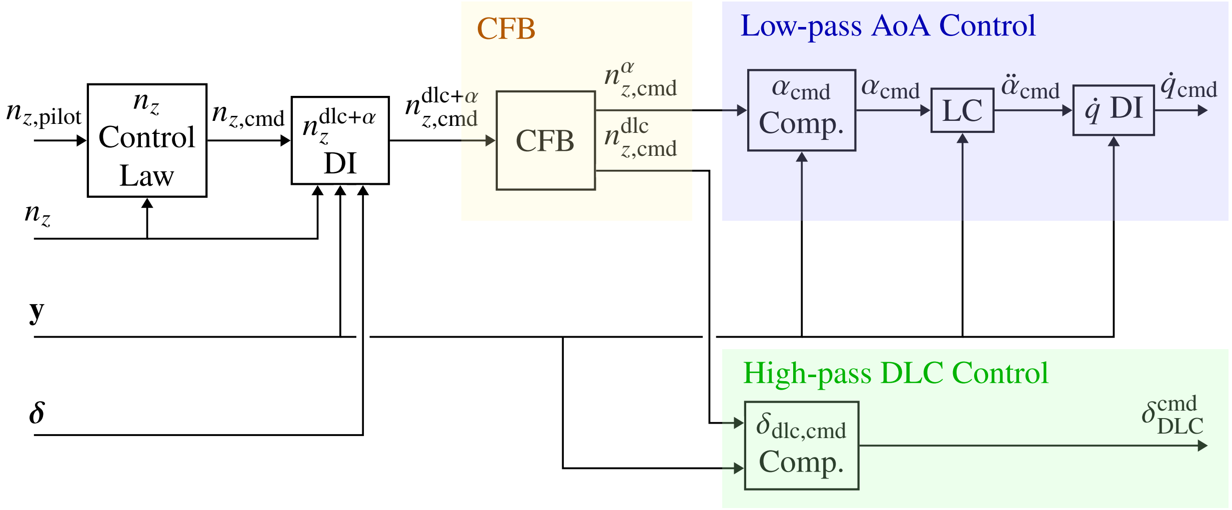

Fig. 4 CFB controller architecture.

Looking at Fig. 4, the CFB is central to the controller architecture. From it, two distinct paths command two different n_z contributions. The high-pass signal commands the DLC control surfaces contribution, while the low-pass signal commands the AoA contribution.

Most of the blocks found in Fig. 4 are equal to the blocks used in the offload architecture. For detailed information on these, see section 4.1. For this CFB architecture, only the "CFB" and "$n_z^{\text{dlc}+\alpha}$ DI" blocks are new.

Given that the CFB splits the input signal into AoA and DLC contributions, this input signal needs to have both contributions: $n_{z,\text{cmd}}^{\text{dlc}+\alpha}$. The block "$n_z^{\text{dlc}+\alpha}$ DI" is responsible for computing this signal. Similar to equation (16), where the total $n_{z,\text{cmd}}$ was used to compute the required DLC contribution, this block does the same thing for both DLC control surfaces and AoA:

$$\begin{aligned} n_{z,\text{cmd}}^{\text{dlc}+\alpha} &= n_{z,\text{cmd}} - \left(n_z - n_z^{\text{dlc}} - n_z^{\alpha}\right) \\ &= n_{z,\text{cmd}} - \left(n_z + \frac{q_\infty}{m_b g}\left(\mathbf{Q}_{z_{\delta_{\text{dlc}}}}\delta_{\text{dlc}} + Q_{z_\alpha}\alpha\right)\right) . \end{aligned} \tag{26}$$

After being computed this $n_{z,\text{cmd}}^{\text{dlc}+\alpha}$ signal is the input for the CFB. The "CFB" block has two functions: split the signal frequency content, and serve as a command filter for the AoA response. The CFB implemented is of second order:

$$n^{\alpha}_{z,\mathrm{cmd}} = \frac{\omega^2_{n,\mathrm{cfb}}}{s^2 + 2\zeta_{\mathrm{cfb}}\omega_{n,\mathrm{cfb}}s + \omega^2_{n,\mathrm{cfb}}} n^{\mathrm{dlc}+\alpha}_{z,\mathrm{cmd}} \tag{27}$$

$$n^{\mathrm{dlc}}_{z,\mathrm{cmd}} = \frac{s^2 + 2\zeta_{\mathrm{cfb}}\omega_{n,\mathrm{cfb}}s}{s^2 + 2\zeta\omega_{n,\mathrm{cfb}}s + \omega^2_{n,\mathrm{cfb}}} n^{\mathrm{dlc}+\alpha}_{z,\mathrm{cmd}} , \tag{28}$$

where $\omega_{n,\mathrm{cfb}}$ is the natural frequency and ζ_{cfb} the damping ratio of the filters. By using the CFB, the intended dynamic behavior is achieved: the DLC control surfaces track the high frequency component of the n_z dynamics, while AoA tracks the low frequency of it. Its crossover frequency is crucial for achieving this, since it determines how AoA and DLC control surfaces are coordinated. Choosing it too high will induce oscillations due to relatively slow AoA dynamics, whereas a low value results in excessive DLC control surface activity.

5 Results

Both these architectures were implemented in a simulation environment for the demonstrator model described in section 3. The four most inboard flaps on each wing were used for DLC purposes. The control allocation vector **A** was chosen to be a column vector of ones, meaning that all DLC control surfaces deflect equally. In section 5.1, the tracking performance of the offload and CFB architectures are presented. Subsequently, in section 5.2, the removal of the non-minimum-phase behavior is analyzed, comparing it with a n_z control architecture without DLC. In section 5.3, disturbance rejection properties are addressed by comparing simulations of the two DLC architectures and the non-DLC architecture in a turbulent wind field. Lastly, in section 5.4, the HiL results are presented. The same simulation scenario presented in section 5.1 was performed with the HiL setup.

To keep the comparison fair between the DLC and non-DLC architectures, an architecture only using the AoA to control n_z was considered. Therefore, the non-DLC architecture uses mostly the same blocks as the proposed DLC architectures with only small changes to them. In particular, a new "n_z^{α} DI" block is introduced, and the parameters of the "n_z Control Law" and "α Command Filter" blocks are adjusted. The architecture is presented in Fig. 5.

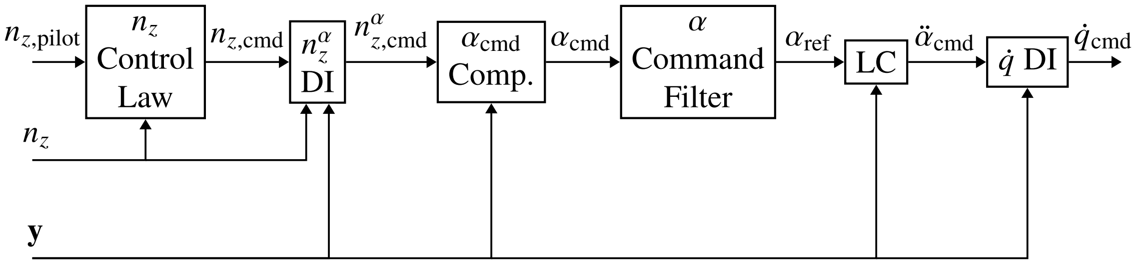

Fig. 5 Non-DLC controller architecture

Given that n_z is tracked using only AoA in this architecture, a "n_z^{α} DI" block is used to compute the AoA commanded n_z contribution. Using similar derivations as equations (16) and (26), the equation implemented in this block is obtained as:

$$n^{\alpha}_{z,\mathrm{cmd}} = n_{z,\mathrm{cmd}} - \left(n_z + \frac{q_\infty}{m_b g} Q_{z_\alpha} \alpha \right) . \tag{29}$$

Regarding parameter changes, the only parameters that were varied were the crossover frequency of the "α Command Filter" block and the n_z control law gain K_{fb}. The crossover frequency was set to a high value of 1.7 rad/s to obtain fast n_z responses while the K_{fb} gain was set to a small value of 0.075 to avoid oscillations.

5.1 Tracking Performance

To evaluate tracking performance, a simulation of the pilot performing a step up followed by a step down command to n_z is performed. The step up is done at 5 seconds and the step down at 15 seconds. The magnitude of it is 0.1 g. This simulation was performed for both the offload and CFB architectures, as shown in Figs. 6–7. In Fig. 6, the normal load factor responses are shown, in Fig. 7 the elevator and DLC control surfaces, and in Fig. 8 the AoA.

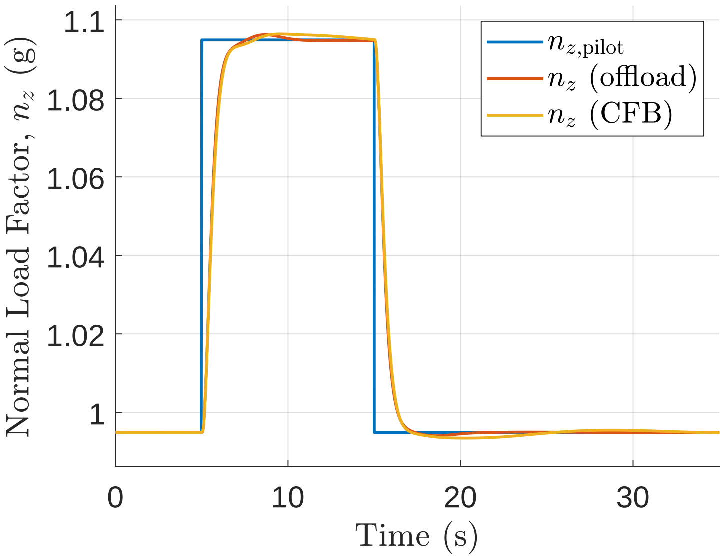

Fig. 6 DLC architectures comparison of n_z responses from a step up and down n_z pilot command simulation.

The n_z responses are fast and track accurately the desired value. There is a small overshoot for the offload architecture mainly due to signal filtering. Although the CFB architecture has an overshoot for the same reason, this architecture originates small non-typical oscillations at the end of the rise time. This indicates a small coupling between the AoA and the DLC control surfaces originating from the CFB. The coupling of the two filtered signals of the CFB is highly dependent on its crossover frequency, as mentioned in section 4.2. Comparing it to the offload architecture, choosing a crossover frequency for the CFB to minimize coupling and achieve adequate coordination was more challenging than choosing an offloading gain K_O. The value used for the CFB crossover frequency was $\omega_{n,\text{cfb}} = 0.6$ rad/s. For the offload architecture, to keep coupling between AoA and DLC control surfaces to a minimum and have a smooth offload of the dynamics, the offloading gain K_O was chosen to be small ($K_O = 0.2$). For both architectures the n_z control law gain K_{fb} was chosen to slightly increase tracking performance and remove n_z steady-state errors. A value of $K_{\text{fb}} = 2$ was chosen for this tunable parameter.

In Figs. 7 and 8, the dynamics of offloading DLC control surfaces to AoA are illustrated. In fact, in Fig. 7 the DLC control surfaces act relatively fast to control the short-term response after a step input, but due to the offloading mechanism the AoA start increasing, taking over the responsibility from the DLC control surfaces, as shown in Fig. 8. As discussed in section 4.1 and 4.2, the DLC control surfaces acting fast, while the elevator and AoA dynamics being slower was the intended behavior. For the offload architecture, this is achieved by the offloading integrator and gain, while for the CFB architecture this is achieved by the CFB and its bandwidth.

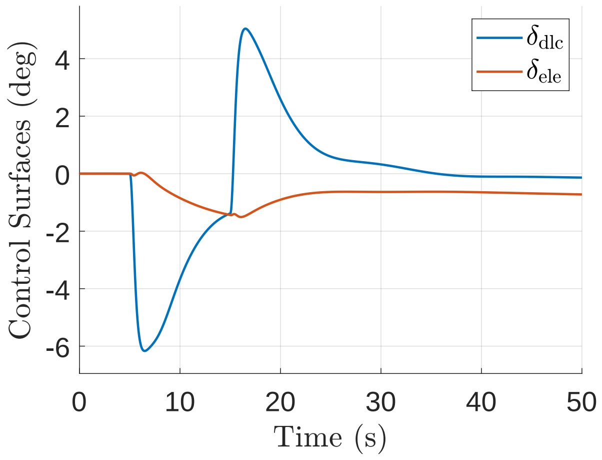

a) Offload architecture **b) CFB architecture**

Fig. 7 DLC architectures comparison of control surfaces responses from a step up and down n_z pilot command simulation.

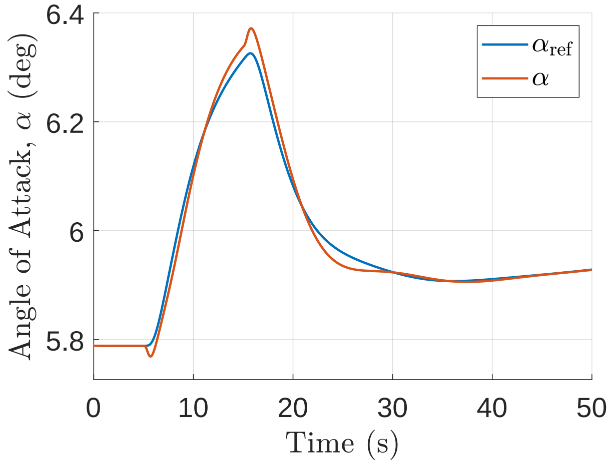

a) Offload architecture **b) CFB architecture**

Fig. 8 DLC architectures comparison of AoA responses from a step up and down n_z pilot command simulation.

Comparing the DLC control surface responses in Fig. 7, the CFB architecture has the advantage of it returning back to zero more accurately when compared to the offload architecture. This happens because of how the offloading integrator is used in its implementation. Assuming the DLC control surfaces to be zero at steady-state for the offload architecture, the signal immediately after the integrator, $n^{\alpha}_{z,\mathrm{cmd}}$, would have to be constant. From equation (19), the commanded AoA is also a function of dynamic pressure. Therefore, changes to dynamic pressure influence the commanded AoA. This is specially relevant when an autothrottle is used, since its ability to track accurately and fast the aircraft's velocity determines if the DLC control surface deflection are offloaded to exactly zero. Therefore, for the offload method, returning the DLC control surfaces back to zero can only happen with a good enough autothrottle that is able to accurately track the desired airspeed. In the CFB architecture, since $n^{\mathrm{dlc}}_{z,\mathrm{cmd}}$ is a high-pass signal, the CFB forces the $\boldsymbol{\delta}_{\mathrm{dlc}}$ to be exactly zero at steady-state.

For improved visualization of the coordination between AoA and DLC control surfaces, Fig. 9 explicitly shows the primary contributors to n_z tracking for both DLC implementations. The normal load factor values are shown in variations from their initial values.

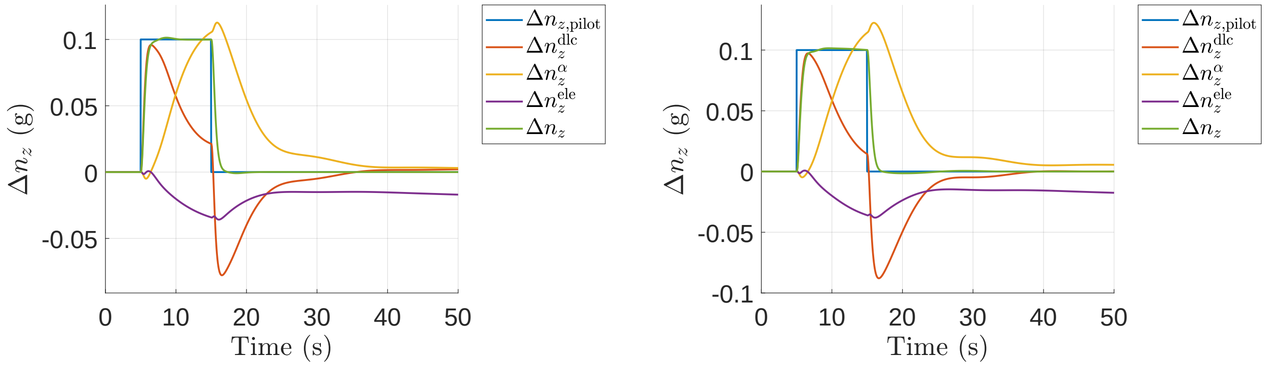

a) Offload architecture **b) CFB architecture**

Fig. 9 Explicit n_z contributions for a simulation of a step up and down n_z pilot command.

Both Figs. 9a and 9b, show the shift in responsibility from DLC control surfaces to AoA and elevators. As illustrated, the n_z^{dlc} contribution acts fast following the step inputs, allowing a quick n_z response. The AoA and elevators follow this fast response by assuming full responsibility of tracking n_z, causing the DLC contribution to return to its initial value. This coordination is crucial for DLC implementations to work and to enable its benefits.

5.2 Non-Minimum-Phase Behavior

One of the aforementioned advantages of DLC is the removal of the non-minimum-phase behavior that comes with the use of elevators. To identify this removal, the zeros of a simpler linear model of the aircraft can be analyzed when the DLC architectures are used in the controller. The linear model in equation (10) is used for these analyses. The open-loop (OL) transfer function from elevators, δ_{ele}, to flight paht angle, γ, is presented in equation (30):

$$\gamma\left(s\right) = \frac{0.061\left(s - 11.44\right)\left(s + 9.675\right)}{s\left(s^2 + 1.774s + 19.78\right)}\delta_{\text{ele}}\left(s\right). \tag{30}$$

From equation (30), the RHP zero $z = 11.44$ can be noted. This is a relatively fast zero that does not impose a limiting bandwidth constraint to the CL system. The high frequency RHP zero is attributed to the aircraft being a relatively small passenger jet and the high airspeed chosen for linearization. Although, the bandwidth constraint does not impose a realistic limitation for the aircraft used in this work, this is rather important for bigger passenger aircraft. Since the goal of this section is to demonstrate the removal of the RHP zero and its bandwidth limitation, the analysis is proceeded with this aircraft and its RHP zero. Assuming a required system bandwidth, ω_{BS}, and a maximum allowed peak, M_S, of the sensitivity function for the CL system, a real RHP zero, z, imposes a bound on ω_{BS} of the form [23, 24]:

$$\omega_{BS} \leq \left(1 - M_S^{-1}\right) z\,. \tag{31}$$

Taking a reasonable maximum allowed peak of $M_S = 2$, the RHP zero of equation (30) imposes a bandwidth limit of $\omega_{BS} \leq 5.72$ rad/s to the controlled system. This is the existent limitation when using only elevators for controlling the vertical dynamics of aircraft. When DLC architectures are considered with proper coordination between elevators and DLC control surfaces, this RHP zero and the bandwidth limitation are removed.

To illustrate the removal of the RHP zero, the zeros of the two DLC architectures, the non-DLC architecture and of equation (30) are displayed in Fig. 10a, and time domain simulations of a step input of $n_{z,\text{pilot}}$ are shown in Fig. 10b for DLC and non-DLC architectures.

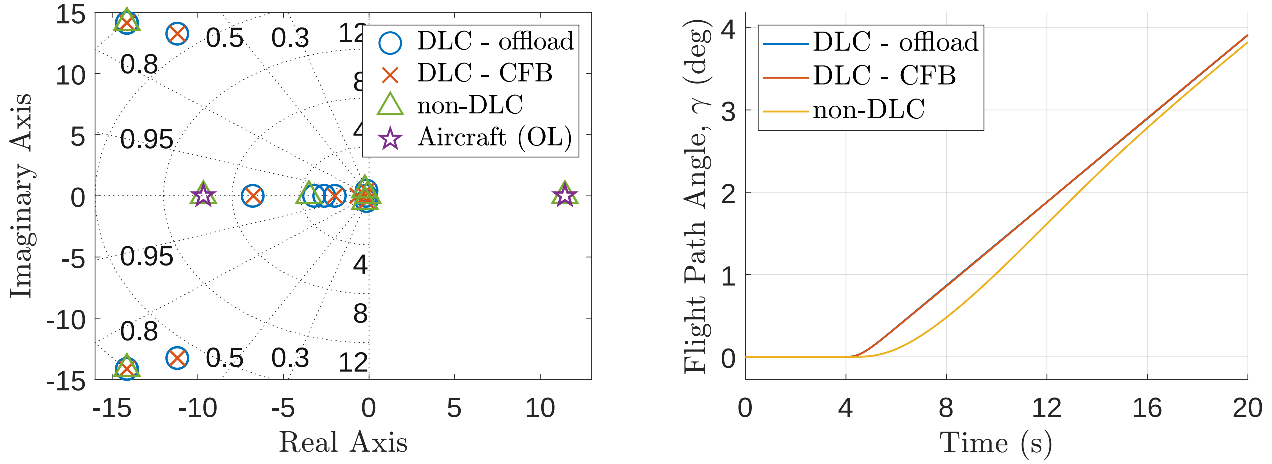

a) Location of zeros in complex plane. **b) γ time response to a $n_{z,\text{pilot}}$ step input.**

Fig. 10 Non-minimum-phase behavior comparison between different controller architectures.

As shown in Fig. 10a, the OL zero remains in the system when using the non-DLC controller architecture. For both DLC architectures, this RHP zero is removed. In Fig. 10b, the flight path angle response for the DLC architectures is significantly faster and directly influenced, whereas the non-DLC architecture exhibits a slower response with non-minimum-phase behavior. For both DLC architectures there is no longer a non-minimum-phase behavior in the CL system. Consequently, the limitation in controller bandwidth for the DLC architectures is eliminated.

5.3 Disturbance Rejection

To address disturbance rejection, a turbulent wind field is considered. The wind field is represented by a Dryden continuous turbulence model. A Total Energy Control System (TECS) is used to track a constant altitude. The TECS implementation described in Ref. [25] is used in this work. The pilot's commanded n_z is replaced by the TECS output. Both DLC and non-DLC architectures are considered and a comparison is made between them when encountering this disturbance. In Fig. 11, simulation results comparing the three architectures are presented. To evaluate disturbance rejection properties, altitude and flight path angle results are displayed in Figs. 11a and 11b. To illustrate the potential pilot workload, the TECS output is shown in Fig. 11c. To address comfort, Fig. 11d shows the pitch angle responses for the three architectures.

From Figs. 11a and 11b, it is evident that the DLC architectures outperform the non-DLC one at handling wind disturbances. As previously mentioned, control architectures with DLC capabilities can reduce altitude and flight path angle variations when encountering these disturbances. Since DLC control surfaces can directly influence lift and more rapidly counteract disturbances to it, disturbance rejection is improved significantly with these architectures. In Fig. 11c, the commanded n_z values from TECS are presented to address the potential pilot workload to maintain the aircraft at constant altitude in turbulent wind fields. The reduction of workload is clear for the DLC architectures. For the non-DLC architecture the oscillations are bigger compared to the required autopilot output of the DLC architectures. Lastly, in Fig. 11d, the pitch angle evolution is shown to analyze comfort levels for passengers. Smaller oscillation amplitudes are desirable to increase passenger comfort. For DLC architectures, pitch oscillations are smaller, performing better for passenger comfort compared to non-DLC architectures.

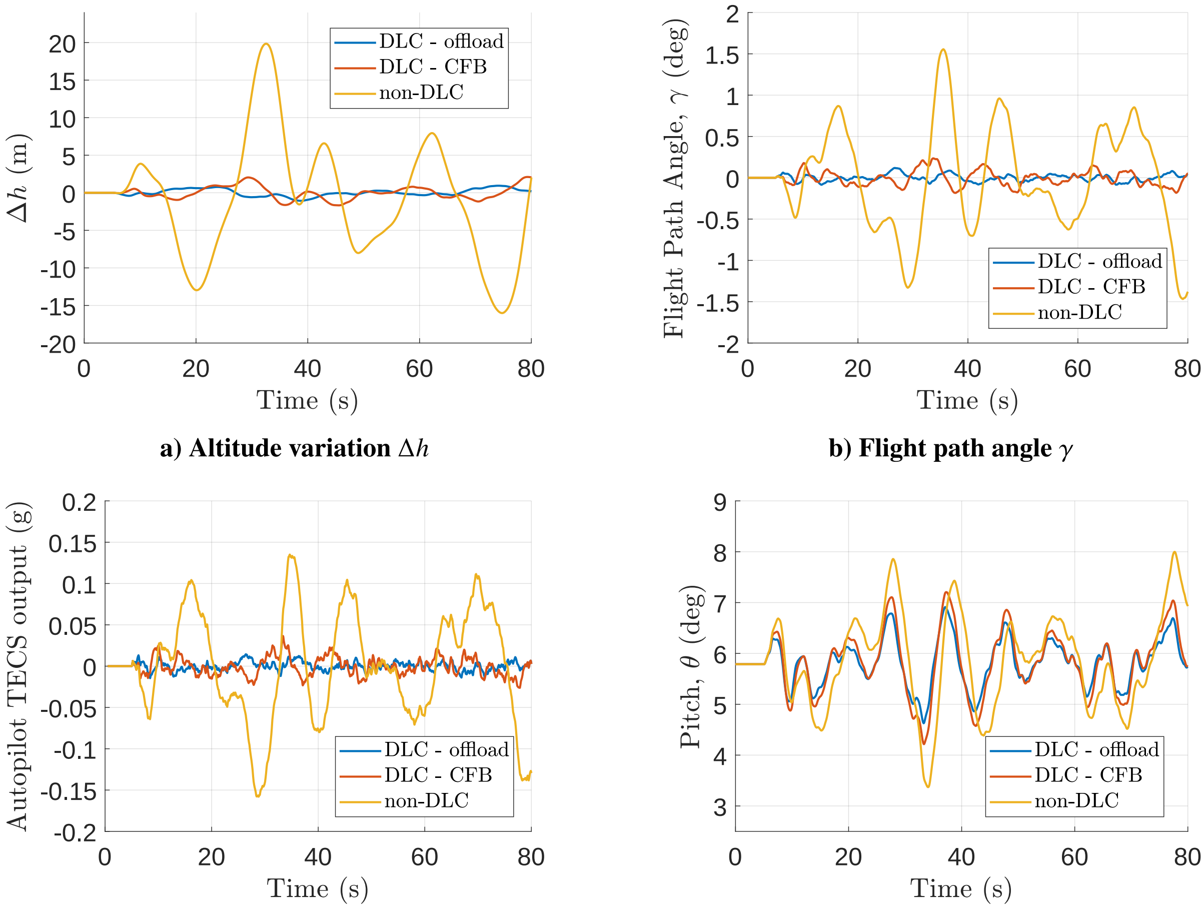

a) Altitude variation Δh

b) Flight path angle γ

c) TECS output from autopilot (n_z)

d) Pitch angle θ

Fig. 11 Comparison between the offload, CFB, and non-DLC architectures under turbulent wind fields.

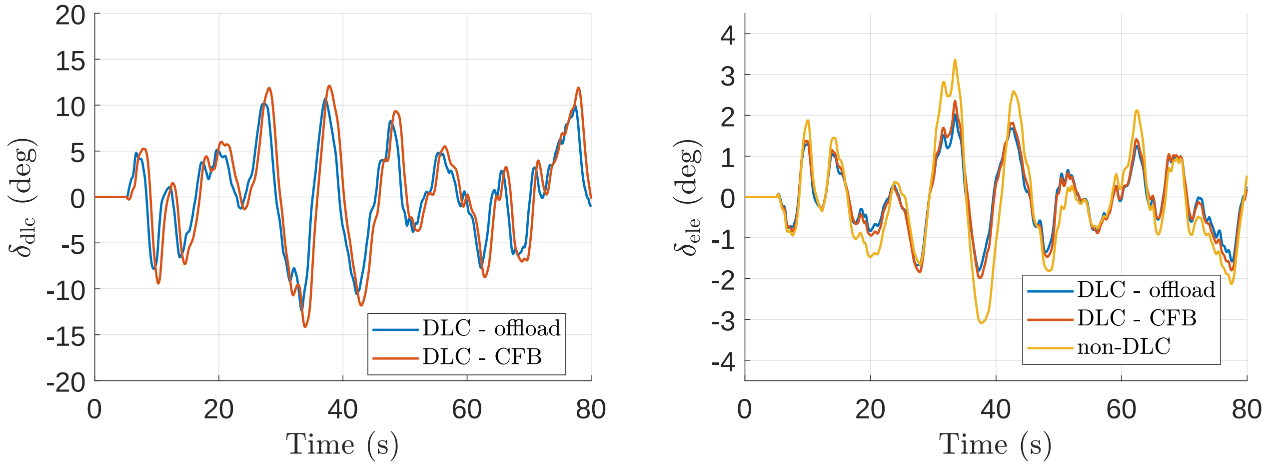

a) DLC control surfaces, δ_{dlc}.

b) Elevators, δ_{ele}.

Fig. 12 Control activity comparison between the offload, CFB, and non-DLC architectures under turbulent wind fields.

In Fig. 11, it was observed that using DLC controller architectures improves significantly disturbance rejection capabilities due to their ability to rapidly counteract perturbation in lift. This ability to counteract disturbances imposes a requirement on control effectiveness of DLC control surfaces, since they try to cancel the disturbances while operating within deflection limits. Fig. 12 shows the control activity under the turbulent wind field.

As illustrated in Fig. 12a, there is some DLC control activity to counteract the wind disturbances. It can also be observed that the DLC control activity for the CFB architecture is slightly greater compared to the offload architecture. This moderate control activity indicates that the control surfaces of this aircraft used for DLC purposes are not highly effective at generating lift. Using equation (7), since the DLC architectures use $\boldsymbol{\delta}_{\text{dlc}}$ to track directly n_z, any AoA disturbance results in $\boldsymbol{\delta}_{\text{dlc}}$ approximately counteracting it:

$$C_{L_\alpha}\alpha_w + C_{L_{\delta_{\text{dlc}}}}\delta_{\text{dlc}} \approx 0. \tag{32}$$

Equation (32) is only an approximation since turbulence effects are introduced into the control law through the measured n_z, which corrects $n_{z,\text{cmd}}$ via an integral term, as shown in Fig.2. To exactly counteract the turbulence effects and to improve the control law, α_w can be estimated and its n_z contribution fed forward negatively in Fig. 2. Nevertheless, when sizing the control surfaces for DLC purposes, equation (32) provides an adequate initial estimate for their control effectiveness based on their maximum allowed deflections. Assuming a worst case disturbance $\alpha_{w,\text{worst}}$ on AoA, and a maximum allowed deflection for DLC control surfaces, $\delta_{\text{dlc,max}}$, the desired $C_{L_{\delta_{\text{dlc}}}}$ can be estimated as:

$$\left|C_{L_{\delta_{\text{dlc}}}}\right| = \frac{\left|C_{L_\alpha}\right|\alpha_{w,\text{worst}}}{\delta_{\text{dlc,max}}}. \tag{33}$$

Equation (33) can be used for preliminary sizing of control surfaces for DLC purposes, or to investigate whether an existing aircraft has the control effectiveness required for implementing DLC capabilities. Taking the aircraft used in this work as an example, assuming a maximum allowed deflection for DLC control surfaces of $\delta_{\text{dlc,max}} = 15$ deg, the allowed worst case disturbance for AoA would be $\alpha_{w,\text{worst}} \approx 1.05$ deg. This worst case disturbance for AoA is rather small, which explains the moderately large deflections obtained for the DLC control activity in Fig. 12a.

5.4 Hardware-in-the-Loop Tests

Hardware-in-the-loop (HiL) testing is a natural step following simulation analyses. To assess the viability of using real control surfaces with a servo actuator for DLC purposes, preliminary HiL tests were conducted. The experimental setup consisted of a test rig to replicate a single MFTE panel and its actuator dynamics. In Fig. 13, an image of the test rig is shown.

The panel is physically connected to an electromechanical servo actuator through a linkage mechanism. With this servo actuator the panel's deflection can be controlled. To simulate the aerodynamic hinge moments acting on the control surface, the panel is physically connected to a pneumatic load actuator. Forces can be commanded to this pneumatic actuator that represent equivalent hinge moments based on aircraft aerodynamics. These represent the two input signals the test rig requires: the commanded panel's deflection and the hinge moment. Additionally, as an output, the test rig has the measured panel's deflection signal which can be fed back to a simulation environment. An in-depth description and characterization of this test rig was performed in [26].

For the HiL tests, the MFTW panel of the test rig was used for representing the DLC control surfaces. Given that the chosen control allocation for these control surfaces deflected them equally, the MFTE panel was used to replace all of the DLC control surfaces. Fig. 14 shows a diagram highlighting the test rig block in red and how it is incorporated into the CL simulation environment. To make it real-time capable, the controller blocks and aircraft had to be linearized to accelerate simulation times.

The same simulation tests presented in section 5.1 were performed with this HiL experimental setup. Given the similarity of the results for the offload and CFB architectures, only the offload architecture results are presented and discussed in this section. Additionally, since the HiL tests were conducted first,

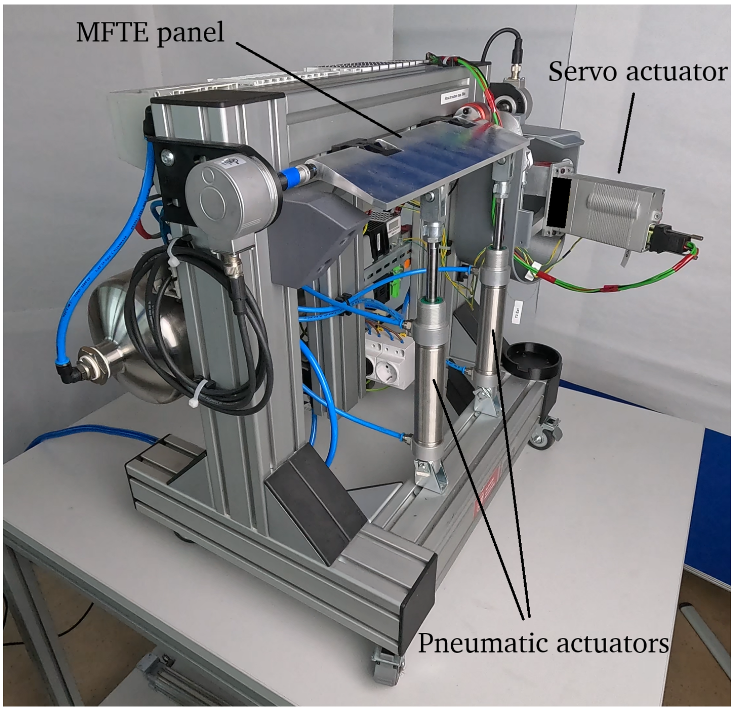

Fig. 13 View of the test rig used for the HiL simulations.

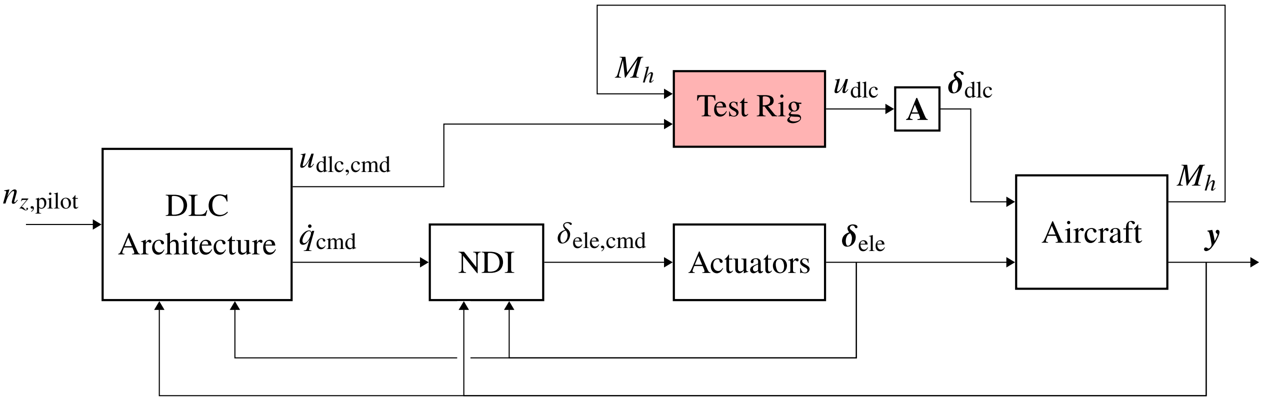

Fig. 14 Vertical dynamics control diagram with HiL setup.

these were performed with an earlier iteration of controller parameters. For the results presented in this section the offloading gain K_O was set to 0.25 and the n_z control law gain K_{fb} to 1. The n_z response result is shown in Fig. 15.

The HiL simulation results have some differences compared to the simulation results in Fig. 6. The triangle-shaped n_z overshoot in Fig. 15 is characteristic for systems containing actuators with free-play. It was noted that the actuation system of the test rig has just over 1 degree of free-play. Additionally, Fig. 15 shows quantization-induced high-frequency oscillations. Both free-play and quantization effects are illustrated in the δ_{dlc} response shown in Fig 16b.

The larger-amplitude, almost discrete variations in Fig 16b correspond to the free-play phenomenon, while the smaller-amplitude variations correspond to quantization. These effects are particularly relevant for DLC implementations given that any disturbance on DLC control surfaces affect directly the n_z response. The δ_{dlc} values in Fig. 16b also exhibit a constant offset from zero due to a non-zero hinge moment applied by the pneumatic actuators. This is undesirable, however, due to how the pneumatic actuators and test rig were setup, it was unavoidable. Additionally, slightly bigger oscillations are

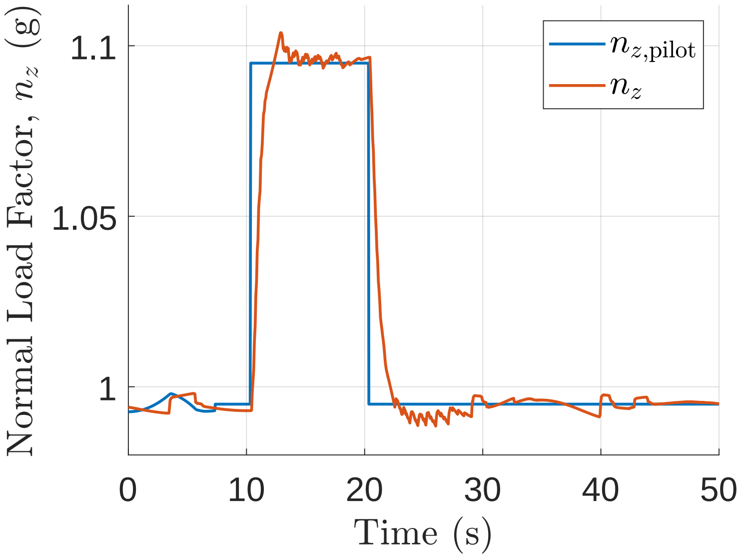

Fig. 15 n_z **response of HiL simulation of a step up and down** n_z **pilot command using the offload architecture.**

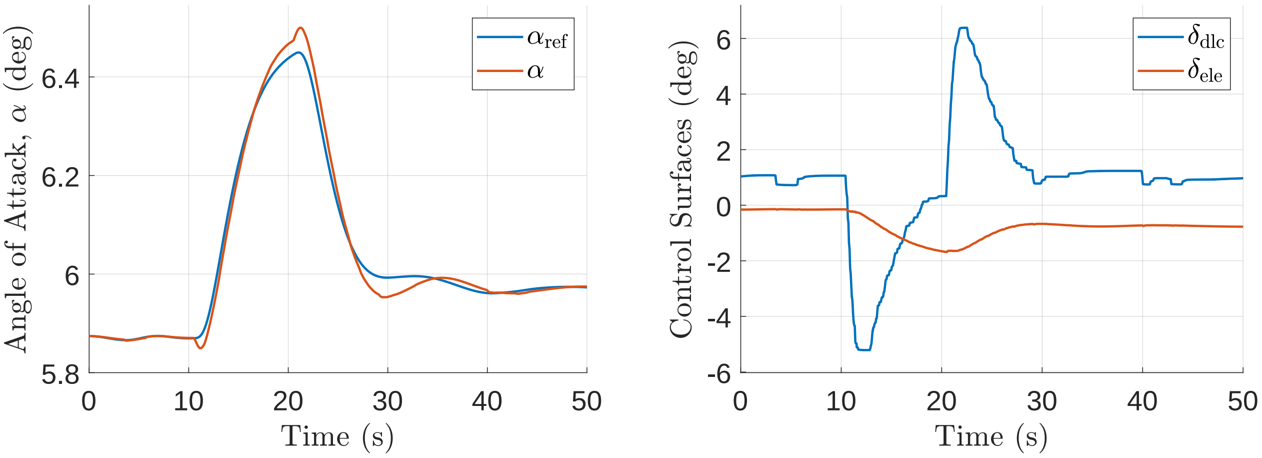

a) AoA, α

b) Control surface deflections

Fig. 16 HiL simulation of a step up and down n_z **pilot command using the offload architecture.**

observed in the AoA response in Fig. 16a when compared to Fig. 8a. These are due to the different value used for the offloading parameter, K_O, in the HiL simulations.

The intended offloading behavior is still present in the HiL tests and is more clearly illustrated by the explicit n_z contributions shown in Fig. 17.

As illustrated, the DLC contribution responds relatively fast and is the primary responsible for tracking the commanded n_z value during the initial seconds, after which it returns to its initial value due to the offloading mechanism, which increases the AoA contribution. The free-play and quantization effects are clearly observed in the DLC contribution. Since these effects are only present in this signal, the oscillations in the total n_z signal are entirely explained by these effects.

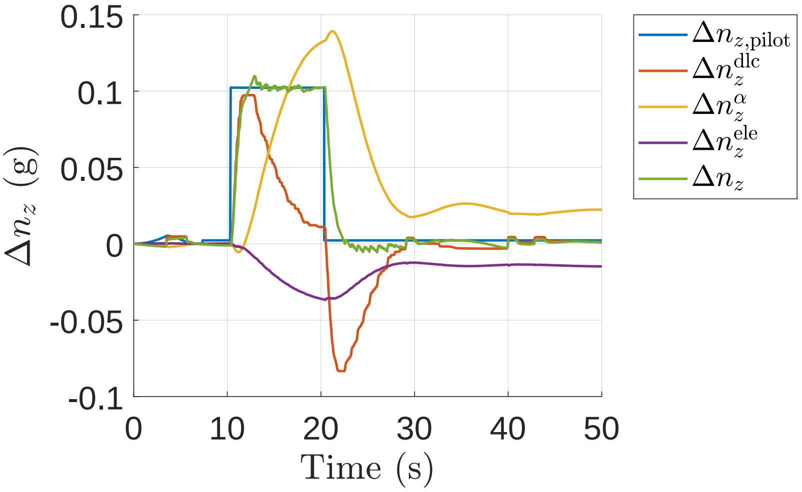

Fig. 17 Explicit n_z contributions for a HiL simulation of a step up and down n_z pilot command using the offload architecture.

6 Conclusions & Future Work

In this paper, DLC architectures were presented and discussed as a promising way of controlling the vertical dynamics of new aircraft concepts. Given that these new aircraft concepts would already have the required MFTE devices, the proposed architectures do not necessitate any hardware changes to the aircraft. Results in the demonstrator model show the benefits of using these approaches.

Both architectures were able to integrate DLC and coordinate it with AoA. Short-term use of DLC control surfaces and long-term adjustment of AoA was achieved. Both architectures show fast normal load factor responses and the successful coordination between AoA and DLC control surfaces. Initial results of the offload architecture show the challenges of returning DLC control surfaces exactly to zero. Since this architecture is able to return the DLC control surfaces to values very close to zero, the tests conducted thus far have not required the development of additional mechanisms to address this non-zero deflections. However, future flight tests may exacerbate this issue, requiring careful consideration of the effects of dynamic pressure and the autothrottle on the offloading mechanism. In contrast, the CFB architecture achieves zeros steady-state deflection values, however, results show small undesirable coupling between the AoA and DLC control surfaces for this architecture. The crossover frequency of the CFB is crucial at coordinating the two and keeping coupling to a minimum.

The typical non-minimum-phase behavior associated with using elevators was also analyzed and results show how the proposed DLC architectures eliminate the RHP zero and the corresponding controller bandwidth limitation. Although for the aircraft considered in this work the upper bound constraint for the bandwidth is large, the constraint becomes crucial for larger passenger aircraft, specially at low airspeeds. These results shows the potential of DLC for improving aircraft handling and disturbance rejection properties.

The disturbance rejection properties were analyzed and compared with a comparable non-DLC controller architecture. Results show the significantly better capabilities of DLC architectures at handling these. Altitude and flight path angle variation were substantially reduced when considering DLC architectures. Additionally, potential pilot workload to maintain constant altitude was assessed using the commanded normal load factor from a TECS function. Results show that pilot intervention is much smaller for the proposed DLC architectures. Passenger comfort levels were also analyzed using the pitch response under the same turbulent wind field. The DLC architectures continued to outperform the non-DLC architecture, leading to greater comfort levels.

DLC control activity was also analyzed using the same turbulent wind fields. Results show the importance of correctly sizing DLC control surfaces. Given its inherit property of counteracting wind disturbances, DLC architectures are only viable if the DLC control surfaces have sufficient control effectiveness. Simple estimations can be computed to quickly assess if an aircraft has the capabilities for DLC implementations or to size DLC control surfaces for new aircraft.

Preliminary HiL results show the feasibility of using real actuation systems for DLC purposes. The results show the effects of free-play and quantization. Although the effects are small they should be properly studied for future flight tests given the direct influence the DLC control surfaces have on the normal load factor.

In-depth synthesis of the parameters used in these architectures to study possible gains in performance will be the focus of future work. Additionally, pilot feedback from piloted tests of these architectures in flight simulators and on the modified Cessna Citation VII aircraft will be implemented and analyzed in the future.

Acknowledgments

This research was funded by the German Federal Ministry for Economic Affairs and Energy (BMWE) under project number 20A2103D (MuStHaF).

Declaration of Use of Artificial Intelligence

Artificial intelligence was not used in the work presented.

References

[1] E. R. Rang. A nonvarying-C* control scheme for aircraft. *Journal of Aircraft*, 8(8):679–680, 1971. doi: 10.2514/3.44293.

[2] E. Field. The application of a C* flight control law to large civil transport aircraft. *College of Aeronautics Report*, 9303, 1993. Available at: `https://dspace.lib.cranfield.ac.uk/items/462304cf-3176-4f46-8f8d-b28ce2e2644c`.

[3] W. J. G. Pinsker. The control characteristics of aircraft employing direct-lift control. Aeronautical Research Council Reports & Memoranda 3629, Royal Aircraft Establishment Aerodynamics Department, 1968. `https://reports.aerade.cranfield.ac.uk/handle/1826.2/2896`.

[4] C. Varriale, T. Lombaerts, and G. Looye. Direct Lift Control: A review of its principles, merits, current and future implementations. *Progress in Aerospace Sciences*, 152(101073), Jan 2025. doi: 10.1016/j.paerosci.2024.101073.

[5] L. O. Lykken and N. M. Shah. Direct lift control for improved automatic landing and performance of transport aircraft. *Journal of Aircraft*, 9(5), May 1972. doi: 10.2514/3.58988.

[6] J. W. Denham. Project MAGIC CARPET:Advanced controls and displays for precision carrier landings. In *54th AIAA Aerospace Sciences Meeting*, San Diego, CA, 2016. doi: 10.2514/6.2016-1770.

[7] R. König, K.-U. Hahn, and J. Winter. Advanced gust management systems: Lessons learned and perspectives. In *AGARD-CP-560, 1995*, 1995. `https://elib.dlr.de/30163/`.

[8] T. Lombaerts and G. Looye. Design and flight testing of nonlinear autoflight control laws incorporating direct lift control. In *Advances in Aerospace Guidance, Navigation and Control*, pages 549–568, Berlin, Heidelberg, 2013. Springer Berlin Heidelberg. doi: 10.1007/978-3-642-38253-6_32.

[9] G. Sim and C. Onspaugh. Laboratory development of selected systems in the lockheed l-1011 tristar. In *3rd Aircraft Design and Operations Meeting, American Institute of Aeronautics and Astronautics*, 1971. doi: 10.2514/6.1971-782.

[10] L. O. Lykken and N. M. Shah. Direct lift control for improved automatic landing and performance of transport aircraft. *Journal of Aircraft*, 9(5):325–332, 1972. doi: 10.2514/3.58988.

[11] Y. Ma and A. Elham. Designing high aspect ratio wings: A review of concepts and approaches. *Progress in Aerospace Sciences*, 145(100983), Feb 2024. doi: 10.1016/j.paerosci.2024.100983.

[12] D. Reckzeh. Multifunctional wing moveables: design of the A350XWB and the way to future concepts. In *29th Congress of the International Council of the Aeronautical Sciences*, 2014. `https://www.fzt.haw-hamburg.de/pers/Scholz/dglr/hh/text_2017_05_04_FluegelA350XWB.pdf`.

[13] C. Varriale. *Flight Mechanics and Performance of Direct Lift Control: Applying Control Allocation Methods to a Staggered Box-Wing Aircraft Configuration*. PhD thesis, Technical University of Delft, Delft, The Netherlands, 2022. doi: 10.4233/uuid:8b868c52-f34f-4307-8fc0-b1176eaf9d04.

[14] D. G. Hull. *Fundamentals of Airplane Flight Mechanics*. Springer Berlin Heidelberg, Berlin, Heidelberg, 2007. doi: 10.1007/978-3-540-46573-7.

[15] J. C. Doyle, B. A. Francis, and A. R. Tannenbaum. *Feedback Control Theory*. Dover, 2009. ISBN: 0486469336.

[16] T. Kier and G. Looye. Unifying manoeuvre and gust loads analysis. In *IFASD 2009*, Seattle, USA, June 2009. `https://elib.dlr.de/97798/`.

[17] Airbus. extra Performance Wing demonstrator takes off, 2023. `https://www.airbus.com/en/newsroom/stories/2023-11-extra-performance-wing-demonstrator-takes-off`.

[18] M. R. Waszak and D. K. Schmidt. Flight dynamics of aeroelastic vehicles. *Journal of Aircraft*, 25(6):563–571, 1988. doi: 10.2514/3.45623.

[19] D. Enns, D. Bugajski, R. Hendrick, and G. Stein. Dynamic inversion: an evolving methodology for flight control design. *International Journal of Control*, 59(1):71–91, 1994. doi: 10.1080/00207179408923070.

[20] D. Bugajski and D. Enns. Nonlinear control law with application to high angle-of-attack flight. *Journal of Guidance, Control, and Dynamics*, 15(3):761–767, 1992. doi: 10.2514/3.20902.

[21] G. Meyer, R. Su, and L. R. Hunt. Application of nonlinear transformations to automatic flight control. *Automatica*, 20(1):103–107, 1984. ISSN: 0005-1098. doi: 10.1016/0005-1098(84)90069-4.

[22] B. L. Stevens, F. L. Lewis, and E. N. Johnson. *Aircraft control and simulation: dynamics, controls design, and autonomous systems*. John Wiley & Sons, 2015. ISBN: 978-1-118-87098-3.

[23] R. H. Middleton. Trade-offs in linear control system design. *Automatica*, 27(2):281–292, 1991. ISSN: 0005-1098. doi: https://doi.org/10.1016/0005-1098(91)90077-F.

[24] S. Skogestad and I. Postlethwaite. *Multivariable feedback control: analysis and design*. john Wiley & Sons, 2005. ISBN: 978-0-470-01168-3.

[25] G. Looye. TECS/THCS-based generic autopilot control laws for aircraft mission simulation. In *EuroGNC 2013, 2nd CEAS Specialist Conference on Guidance, Navigation & Control,*, June 2013. `https://elib.dlr.de/83741/`.

[26] P. Heinrich, P. Meyer, E. Brokof, C. Naue, and C. Hühne. Electric drive systems for multifunctional trailing-edge control surfaces: Dynamic and thermal characterization under simulated flight loads. *Aerospace Science and Technology*, 168:110824, 2026. ISSN: 1270-9638. doi: https://doi.org/10.1016/j.ast.2025.110824.